RESEARCH ON THE IDENTIFICATION AND CONDITION ASSESSMENT OF SURFACE CRACKS IN WESTERN MINING AREAS BASED ON DRONE INFRARED IMAGING

by

Yang CHENG *

China Energy Shendong Coal Group Co., Ltd,
Ecological Environment Management Center, Ordos, Inner Mongolia, China

Original scientific paper
https://doi.org/10.2298/TSCI2502049C

Mining-induced ground fissures can lead to significant subsidence, causing serious damage to the ecological environment of mining areas. This study developed a drone and infrared camera system for fissure detection by using image processing techniques. The main conclusions are: collecting infrared images during periods of significant temperature difference yields better monitoring results for mining-induced fissures, particularly from 10:50 a. m. to 2:50 p. m, by calculating convolution, the temperature gradients in infrared images can be effectively delineated, allowing for more accurate identification of fissure locations, and the temperature variations of surface fissures are influenced by specific heat capacity and thermal convection, with the thermal convection between the air inside the fissures and the ambient air.

Key words: *mining area, ground fissures, infrared imaging, monitoring system, fissure condition assessment*

Introduction

The western region is one of China's primary coal-producing areas, the raw coal output from Inner Mongolia, Shanxi, Shaanxi, and Xinjiang accounts for approximately 75% of the country's total. The issue of surface subsidence has become increasingly severe, and occurrences of ground fissures have become more frequent. It has significantly heightened the challenges of environmental protection, and severely impacted residential safety and farmland development [1-3]. Therefore, early identification and detection of ground fissures in these high risk mining areas is of utmost importance.

Currently, various methods are available for identifying surface fissures, predominantly relying on manual surveys. The time-consuming and costly nature of manual monitoring restricts its application over large areas and complex terrains [4, 5]. Synthetic aperture radar interferometry (InSAR/SAR) enables large-scale, high precision monitoring of surface subsidence, allowing for the inversion of data to obtain subsidence measurements and small-scale fissure deformation [6]. Prush and Lohman [7] determined the time series of elevation changes caused by mining at the Centralia coal mine in Washington State using satellite radar and optical imagery, exploring methods to reduce potential biases. Recently, the rapid development of drone technology has provided new solutions for fissure monitoring [8]. Drones equipped with infrared cameras can efficiently capture surface temperature information, as fissure areas typi-

* Author's e-mail: 20029910@ceic.com

cally exhibit significantly different temperature characteristics compared to their surroundings [9]. Utilizing infrared imaging technology allows for precise identification of fissure locations and conditions, enhancing both the efficiency and accuracy of monitoring data.

This paper aims to explore effective algorithms and techniques for identifying ground fissures using drones equipped with infrared cameras. Through systematic data processing and analysis, this research seeks to provide a scientific basis for safety management and risk assessment in mining areas, while also supporting sustainable development efforts in the sector.

Construction and principles of the monitoring system

Given that the monitoring targets are ground fissures caused by mining in the western regions, which are primarily distributed in open outdoor areas, drones are well-suited for effective identification and monitoring in such expansive environments. The monitoring system consists of two main components: the drone and the camera. For infrared observation of surface fissures and modelling of the 3-D terrain, a DJI M600 Pro six-rotor drone is used, equipped with a Tau2-640R high definition infrared camera.. The camera is positioned on the underside of the drone, allowing for controlled flight over the target mining area to monitor and identify fissure boundaries and morphological characteristics. The drone's camera captures images of the surrounding environment, and the thermal imaging results from the infrared camera are used to generate 3-D cloud maps, effectively illustrating the specific parameters of the ground fissures, as shown in fig. 1.

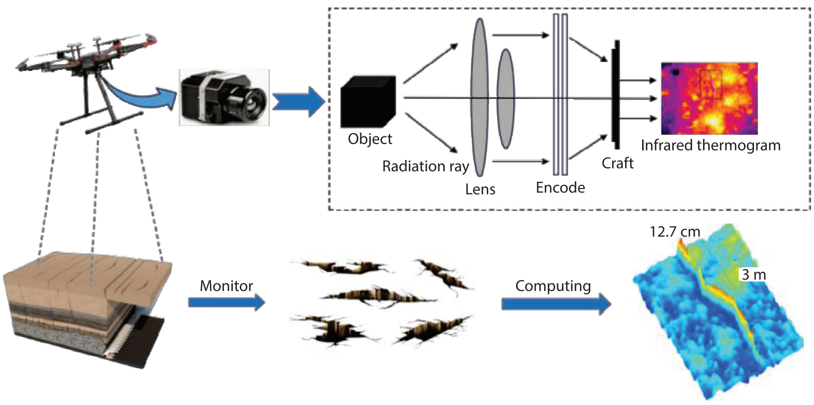

Figure 1. Monitoring platform system and workflow

Principle of infrared monitoring

Infrared imaging technology generates images by capturing infrared radiation emitted by objects. Since all objects emit infrared radiation when their temperature is above absolute zero, the radiation is converted into electrical signals by detectors. These signals are then focused through an optical system, and the processed signals are used to create visual images. Surface cracks, which extend deep into the ground, cause a significant temperature difference between the crack surface and the surrounding ground surface. This temperature variation results in distinguishable differences in the infrared radiation emitted by the cracks and the ground.

Flight parameters and route planning

To determine the drone's flight path, image control points need to be uniformly arranged based on the topographic variations of the ground area. The drone is then controlled to fly back and forth along these image control points until complete image coverage of the entire study area is achieved. On October 23, 2023, an aerial survey was conducted over the entire surface above the coal mining face. During this process, key flight parameters were obtained using DJI GS PRO software: flight altitude of 150 m, front overlap of 70%, side overlap of 65%, and a shutter interval of 2 seconds.

To capture optimal images of surface cracks caused by mining activities, a drone equipped with a high definition infrared camera and a visible light camera was used to observe a fixed crack area above the 12401 working face. The observations were conducted on a spring day, with an interval of two hours between observations. The drone flew at an altitude of 15 m, and a total of 12 sets of infrared images and six sets of visible light images of the study area were collected at different times. The target observation area was selected directly above the working face after 238 m of advancement. A square area of approximately 6 m × 6 m was outlined with lime, and a square reference marker of 45 cm × 45 cm was drawn in one corner for size reference.

Data processing and analysis

Image preprocessing

The infrared images captured by the drone are imported from the device to a computer for an initial inspection ensure data completeness and that the quality meets analysis requirements. During the image acquisition process, infrared images may be affected by noise, such as thermal noise and environmental noise. Gaussian filtering can be applied to remove noise while preserving critical crack information. The Gaussian filtering process is described [3, 4]:

$$I_{filtered}\left(x,y\right)=\frac{1}{2\pi\sigma^2}\sum_{i=-k}^{k}\sum_{j=-k}^{k}I\left(x-i,y-i\right)\mathrm{e}^{-\frac{i^2+j^2}{2\sigma^2}} \tag{1}$$

where $I(x, y)$ is the pixel value of the image, σ – the standard deviation of the Gaussian filter, and k – the size of the filter kernel.

Crack detection algorithm

Edge detection is a crucial step in identifying cracks in infrared images, as cracks typically appear as narrow, low temperature regions. The Sobel operator edge detection algorithm is used to identify these elongated features by calculating the gradient in each direction through convolution operations.

The horizontal and vertical gradients G_x, G_y are expressed [5]:

$$G_x=\begin{bmatrix}-1 & 0 & 1\\ -2 & 0 & 2\\ -1 & 0 & 1\end{bmatrix}I\left(x,y\right) \tag{2}$$

$$G_y=\begin{bmatrix}-1 & -2 & -1\\ 0 & 0 & 0\\ 1 & 2 & 1\end{bmatrix}I\left(x,y\right) \tag{3}$$

The gradient magnitude $|G|$ and gradient direction θ are calculated [5]:

$$\left|G\right|=\sqrt{G_x^2+G_y^2} \tag{4}$$

$$\theta=\arctan\left(\frac{G_y}{G_x}\right) \tag{5}$$

The gradient magnitude $|G|$ can be used for edge detection, while the direction θ can be applied to further optimize the crack contours.

Due to the temperature difference between the crack areas and the surrounding surface, temperature gradient analysis can further confirm the location and shape of the cracks. By analyzing the temperature distribution in the images, abrupt changes and areas with the largest temperature differences can be identified, supporting the edge detection results and eliminating false detections in non-crack regions. The temperature gradient in infrared images can be calculated by analyzing the temperature variation at each pixel [6]:

$$T_{\text{gradient}}\left(x,y\right)=\sqrt{\left(\frac{\partial T}{\partial x}\right)^2+\left(\frac{\partial T}{\partial y}\right)^2} \tag{6}$$

where T is the temperature value at each pixel in the image. Areas with a large temperature gradient typically correspond to crack locations.

Crack condition assessment

The length and width of the identified cracks are measured, and the geometric characteristics of each crack are recorded to assess their development. The width of the crack is calculated by measuring the distance between pixels. If the spatial resolution of the image is r (the actual distance represented by each pixel), then the crack width, W, can be expressed [8]:

$$W = n \times r \tag{7}$$

where n is the number of pixels spanning cracks and r – the spatial resolution of the image.

By combining multi-view images with a digital elevation model, a 3-D reconstruction method is employed to estimate the crack depth. The formula for estimating the depth, D [8]:

$$D=\frac{b\times f}{d} \tag{8}$$

where b is the baseline distance between the two viewpoints, f – the focal length of the camera, and d – the disparity, which is the difference in the observed position of the same point from the two perspectives.

Using the data collected from multiple flights, a geospatial cloud map of the target area is constructed, and the crack width and depth are determined using the aforementioned formulas. Active cracks typically exhibit periodic temperature fluctuations or significant temperature differences. By comparing the current data with historical data, the cracks can be evaluated for trends of expansion, widening, or lengthening, allowing the identification of active cracks that may pose potential risks.

Results and discussions

The actual surface temperature may differ from the temperature observed in infrared images. Therefore, in addition capturing infrared images, a handheld thermometer was used to measure the real-time temperature of surface cracks, aeolian sand, and air. The temperature evolution of these objects over time is shown in fig. 2. It can be observed that the highest surface temperature occurs at 12:50 p. m., reaching 48. 1 °C, which corresponds to the time of maximum solar radiation. In contrast, the highest temperature in the surface cracks lags behind, occurring at 2:50 p. m. with a peak temperature of 39.1 °C.

The temperature variation of objects is related to their specific heat capacity. Aeolian sand, having a relatively low specific heat capacity, experiences larger temperature changes under the same heat radiation exposure. On the other hand, the temperature of surface cracks remains lower and changes less significantly due to the heat convection between the air inside the cracks and the outside air. Between 12:50 a. m. and 4:50 a. m., as there is no external heat source, the temperature of aeolian sand continues to drop. Meanwhile, the surface cracks maintain a temperature 2-3 °C higher than that of the aeolian sand, due to the thermal convection between the warm air within the cracks and the cooler surface air.

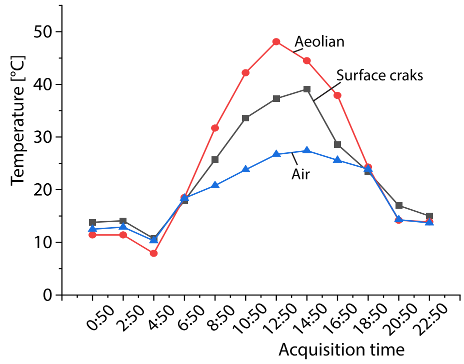

Figure 2. Temperature evolution curves

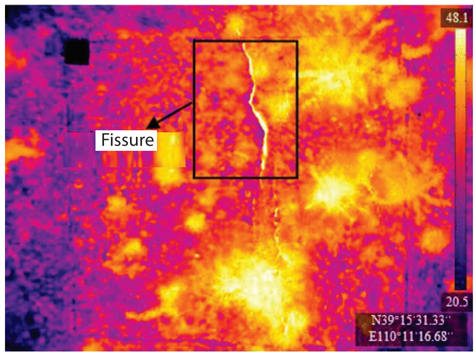

Figure 3. Infrared thermal image

Six sets of temperature images of surface cracks were captured at different times using a drone equipped with an infrared camera. Among these images, the one showing the greatest temperature difference between the surface and the cracks was selected for crack identification, as shown in fig. 3. Gaussian denoising was applied to the image to obtain a high definition picture. The Sobel operator was then utilized for edge detection identify the crack boundaries. Convolution calculations were performed to obtain the temperature gradients in both the horizontal and vertical directions, enhancing the visibility of the crack's temperature features.

From fig. 3, it is evident that the crack is located in the upper portion of the image, indicated by a black rectangle. By proportionally converting the pixel size of the image, the length of the crack was determined to be 3 m, and the width was found to be 12.7 cm.

Conclusion

Drone-based infrared technology can effectively monitor surface cracks induced by mining activities, offering a more efficient and cost-effective solution. Infrared images captured during midday, particularly between 10:50 a. m. and 2:50 p. m., are more conducive to identifying mining-induced cracks. By calculating the convolution, the temperature gradients of infrared photos can be delineated, allowing for a more accurate identification of crack locations. The Sobel operator is employed to delineate the edges of the cracks, enabling the extraction of specific characteristic parameters of the cracks. The temperature variations of surface cracks are influenced by specific heat capacity and heat convection, revealing the differences in temperature responses of various objects under the same thermal radiation conditions.

Nomenclature

b – baseline distance, [m]
D – crack depth, [mm]
d – difference in the observed position, [m]
f – focal length of the camera, [m]
G – gradient, [–]
I – pixel value of the image, [–]
T – temperature value, [°C]
W – crack width, [mm]

Greek symbols

θ – gradient direction, [–]
σ – standard deviation of the Gaussian filter, [–]

References

[1] Malinowska, A. A., Hejmanowski, R., The Impact of Deep Underground Coal Mining on Earth Fissure Occurrence, *Acta Geodynamica Et Geomaterialia*, *4* (2016), 1, pp. 321-330
[2] Teng, T., *et al.*, Overburden Failure and Fracture Propagation Behavior under Repeated Mining, *Mining Metallurgy and Exploration*, *42* (2025), 4, pp. 219-234.
[3] Zhu, J. H., *et al.*, Development Characteristics and Formation Analysis of the Liangjia Village Earth Fissure in the Weihe Basin, China, *Frontiers of Earth Science*, *14* (2020), 2, pp. 758-769
[4] Zhao, H., *et al.*, Monitoring and Mechanisms of Ground Deformation and Ground Fissures Induced by Cut-and-fill Mining in the Jinchuan Mine, *Environmental Earth Sciences*, *68* (2013), 2, pp. 1903-1911
[5] Teng, T., *et al*., Experimental and Numerical Validation of an Effective Stress-sensitive Permeability Model under Hydromechanical Interactions*, Transport in Porous Media*, *151* (2024), 3, pp. 449-467
[6] Zhao, C., *et al.*, Different Scale Land Subsidence and Ground Fissure Monitoring with Multiple InSAR Techniques over Fenwei Basin, Prevention and Mitigation of Natural and Anthropogenic Hazards, *Land Subsidence*, *2* (2015), 3, pp. 305-309
[7] Prush, V. B., Lohman, R. B., Time-Varying Elevation Change at the Centralia Coal Mine in Centralia, Washington (USA), Constrained with InSAR, ASTER, and Optical Imagery, *IEEE Journal of Selected Topics in Applied Earth Observations and Remote Sensing*, *8* (2015), pp. 919-925
[8] Zhang, F., *et al*., A New Identification Method for Surface Cracks from UAV Images Based on Machine Learning in Coal Mining Areas, *Remote Sensing*, *10* (2020), 2, ID1571
[9] Zhao, Y. X., *et al.*, Heat Transfer and Temperature Evolution in Underground Mining-induced Overburden Fracture and Ground Fissures: Optimal Time Window of UAV Infrared Monitoring, *International Journal of Mining Science and Technology*, *34* (2024), 3, pp. 31-50

Paper submitted: August 18, 2024
Paper revised: September 10, 2024
Paper accepted: October 11, 2024